Volume 17, Issue 3, 172520 (1-17)

Iranian Journal of Earth Science (IJES)

https://doi.org/10.57647/j.ijes.2025.16786

Comparative analysis of Permian-Triassic sequences in the eastern Persian Gulf: insights into their paleoenvironments and diagenetic history

Mehrdad Shahkaram[1], Mohsen Aleali[1], Vahid Tavakoli[2,*], Zahra Maleki[1]

[1]*Department Earth Sciences, Science and Research Branch, Islamic Azad University, Tehran, Iran.*
[2]*School of Geology, College of Science, University of Tehran, Tehran, Iran.*

[*]**Corresponding author:** vtavakoli@ut.ac.ir

Review Paper

Received:
20 January 2024
Revised:
11 March 2024
Accepted:
18 May 2024
Published online:
10 July 2025

Abstract:

The Late Permian-Early Triassic Upper Dalan Member and Kangan Formation form one of the richest and most important hydrocarbon reservoirs in the Persian Gulf. To investigate the paleo-depositional environments and sequence stratigraphy of this carbonate-evaporite sequence, two wells (labelled here as A and B) were selected from two oil fields in the eastern part of the Persian Gulf. A total of 15 carbonate microfacies have been identified in a carbonate ramp setting, sloping towards the northeast. The diagenetic history of the succession includes marine, meteoric, and shallow and deep burial diagenesis. Dissolution and dolomitization enhanced the reservoir quality, whereas calcite and anhydrite cementation along with mechanical compaction significantly reduced the reservoir properties. Five third-order depositional sequences were determined using the transgressive-regressive model. Three third-order depositional sequences were identified in the Upper Dalan Member, along with two third-order depositional sequences in the Kangan Formation. An erosional unconformity separates the Upper Dalan Member and Kangan Formation, which coincides with the boundary of the Permian and Triassic strata. This boundary is associated with a major global relative sea-level fall, which has yielded major effects on sediments.

Keywords: Persian Gulf; Upper dalan member; Kangan formation; Carbonate ramp; Sequence stratigraphy

1. Introduction

The Late Permian to Early Triassic depositional succession represents the most significant reservoirs of non-associated natural gas in the Persian Gulf (Al-Husseini and Koehrer, 2013). During that time, the Upper Dalan Member and the Kangan Formation in the Zagros Basin and their correlatable unit in Saudi Arabia and the United Arab Emirates, the Upper Khuff Formation, were deposited in a shallow carbonate platform under hot and dry climate conditions (Alsharhan, 2006; Naderi-Khujin and Tavakoli, 2023). The widespread distribution of depositional facies is related to the relative sea-level change and can be accurately predicted through a comprehensive understanding of these facies' patterns. The relative sea-level changes resulted in variations in depositional and diagenetic processes. It affected the stacking pattern of depositional facies and the type and intensity of the early diagenetic processes. Therefore, to better understand the depositional facies and provide an accurate conceptual model, it seems necessary to study depositional systems and sedimentary sequences. Depositional successions are formed under the influence of the relative sea-level changes, which are controlled by the tectonics of the region and climate conditions. Due to the importance of the reservoir units of this huge hydrocarbon basin, extensive studies have provided a large database on biostratigraphy, depositional environment, and sequence stratigraphy of these formations (Insalaco et al., 2006; Amel et al., 2015; Mehrabi et al., 2015; Rezavand et al., 2017; Kakemem et al., 2021). In addition, the effect of diagenetic processes and depositional facies on reservoir characteristics was analyzed by different researchers (Rahimpour-Bonab et al., 2014; Abdolmaleki and Tavakoli, 2016; Nazari et al., 2019; Jehangir Khan et al., 2021; Ghasemi et al., 2022; Nafisi and Tavakoli, 2023). Insalaco et al. (2006) investigated the regional sedimen-

tology, biostratigraphy, and sequence stratigraphy of the Late Permian-Early Triassic strata in the Kuh-e Surmeh and Kuh-e Dena sections of the Zagros Mountains, and their equivalent in the offshore Fars subsurface. They found four third-order and nine fourth-order sequences in these deposits. Alsharhan (2006) identified the depositional characteristics and hydrocarbon parameters of the Khuff Formation in Abu Dhabi, Dubai, and the north of the United Arab Emirates (UAE). Based on the latter study, 10 microfacies related to lagoon, shoal, shallow shelf environments, and seven third-order depositional sequences were identified. Using petrographic and geochemical analyses, Tavakoli et al. (2018) identified an unconformity between Upper Dalan Member and Kangan Formation in the central Persian Gulf. The sea-level fall during the end of the Permian coincided with a global extinction event (Huang et al., 2019; Zhao et al., 2021), at which various biological species vanished (Haghighat et al., 2020). The Kangan Formation is overlain by the Dashtak Formation (Fig. 2). The global carbon cycle and increased CO_2 levels, geochemical changes in the seawater, meteorite collisions, and extreme climate changes are among the reasons mentioned for the end-Permian mass extinction (Heydari et al., 2001; Berner, 2002; Heydari et al., 2008; Ying et al., 2017; Maaleki-Moghadam et al., 2019; Saitoh and Isozaki, 2021).

This study aims to compare the facies changes and the effect of diagenetic processes concerning the relative sea-level changes in the Upper Dalan Member and the Kangan Formation in two wells (A and B) belonging to two oil fields located east of the Persian Gulf (Fig. 1). The results of this study will be used as the main part of the industrial development programs and the research associated with increasing the production recovery for the Upper Dalan Member and Kangan Formation in the eastern part of the Persian Gulf. In the upper Permian and lower Triassic strata, transgressive–regressive (T-R) depositional sequences have been identified and correlated with regional and global studies (i.e., (Sharland et al., 2001; Al-Husseini and Koehrer, 2013; Rezavand et al., 2017)). This study aims to improve the understanding of regional facies distribution within the basin, offering valuable insights for petroleum system analysis in this area.

2. Geological setting

The Persian Gulf is one of the richest hydrocarbon-producing sedimentary basins in the world. The Permian-Triassic succession is the main target for the exploration of gas and condensates, and giant gas reservoirs have been discovered in this basin (Bashari, 2005; Asadi-Eskandar et al., 2013; Abdolmaleki and Tavakoli, 2016; Naderi-Khujin et al., 2016b, 2016a; Jodeyri-Agaii et al., 2018; Jamalian and Tavakoli, 2022; Mohsin et al., 2023; Shabani et al., 2022; Shabani et al., 2023). The evolution of this sedimentary basin coincided with the separation of parts of Iran from the Arabian Plate and the extension of the Neo-Tethys, in the inactive northeast margin of the Arabian Plate (Sharland et al., 2001; Sharifi-Yazdi et al., 2019; Sharifi-Yazdi et al., 2020; Davoodi et al., 2024).

At the beginning of the middle Permian, the Neo-Tethys ex-

Figure 1. Location map of the study area in the eastern Persian Gulf basin.

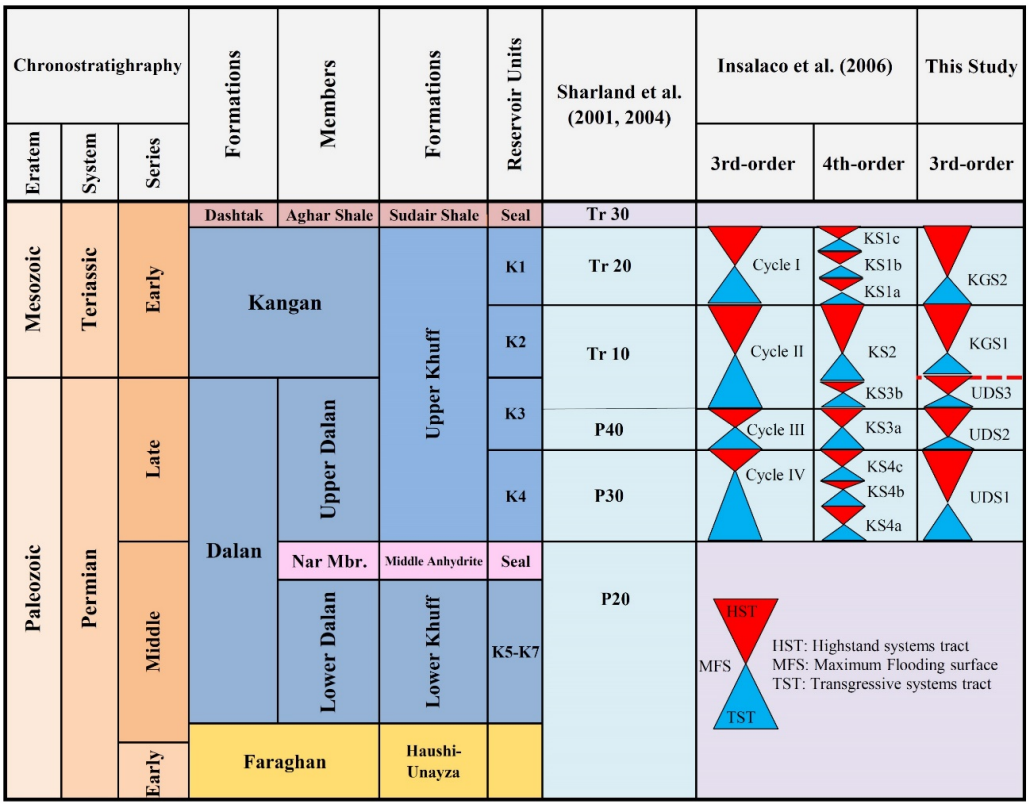

Figure 2. Lithostratigraphic chart of the Upper Dalan Member and the Kangan Formation in the studied fields (Modified after (Insalaco et al., 2006)).

tension and transgression provided accommodation space. The Faraghan Formation was covered by the carbonate-evaporite deposits of the Dalan Formation. The Dalan Formation exists across a substantial portion of the Zagros Basin. This formation includes three members: the Lower Dalan, the Nar evaporites, and the Upper Dalan. With a new transgression of the sea in the Early Triassic, the Kangan Formation covered the sediments of the Dalan Formation giving rise to a discontinuous boundary (Abdolmaleki and Tavakoli, 2016). The Kangan Formation consists of dolomite and limestone deposits with evaporite interlayers and is overlain by the Dashtak Formation. The contact with the Dashtak Formation is conformable (Szabo and Kheradpir, 1978). The Upper Dalan Member and Kangan Formation are known as a heterogeneous carbonate-evaporite reservoirs (Hosseinzadeh and Tavakoli, 2025) in which various facies and diagenetic processes control the reservoir quality (Tavakoli, 2021). The Upper Dalan Member consists of two reservoir units including K4 (limestone and dolomite with some anhydrite) and K3 (dolomite with lime and anhydrite interlayers). The Kangan Formation is composed of two reservoir units namely K1 and K2. They consist of dolomite and limestone interbedded with evaporites (Fig. 2).

3. Materials and methods

This study is based on data obtained from two wells labelled here as A and B, from two oil fields in the eastern part of the Persian Gulf. A total of 2207 microscopic thin sections from the drilling core with a sampling interval of about 25 cm from the Upper Dalan Member and the Kangan Formation (well A: 1110 and well B: 1097 thin sections) were studied. The microfacies, grain size, abundance of allochems, and sedimentary texture as well as diagenetic processes have been determined by petrographic studies. Dunham (1962)'s classification of carbonate rocks was used to categorize facies and sedimentary textures.

To differentiate between calcite and dolomite, thin sections were stained with alizarin red solution according to Dickson (1965)'s method. The concepts of sequence stratigraphy, progradation-retrogradation processes, and main stratigraphic surfaces have been determined based on the evaluation of depositional facies and determination of facies associations, using the model of Embry and Johannessen (1993).

4. Results

4.1 Facies analysis

Based on petrographic studies, 15 microfacies were identified and grouped in four facies associations (tidal flat, lagoon, shoal, and open marine) (Table 1).

4.1.1 Tidal flat facies association

This facies association consists of layered to nodular anhydrite, dolo-mudstone with anhydrite nodules, dolo-mudstone with fenestral fabric, stromatolite boundstone, thrombolite boundstone, and peloidal intraclastic packstone.

4.1.1.1. Layered to nodular anhydrite (MF1)

This facies is composed mainly of layered and nodular anhydrites with parallel and sub-parallel, radial, needle-shaped crystals (Fig. 3 (a)). The abundance of anhydrites is more than 90% and the thickness of this facies is less than 0.8 meters. The abundance of these microfacies in wells A and

Table 1. microfacies description and facies associations in the studied wells.

Microfacies code	microfacies name	Thin-section photograph	Depositional texture and grain type	Diagenetic alteration	Porosity type	facies association
FM1	Layered to nodular anhydrite	Figure 3a	Nodular fabric and layered, Anhydrite crystal shape varies from parallel to sub parallel and radial to a combination of needle shaped	-	-	Tidal flat
FM2	Dolo-mudstone with anhydrite nodules	Figure 3b	Nodular fabric and chicken-wire texture, dolomite crystals are xenotopic to hypidiopic	Dolomitization and pore filling/pervasive anhydrite cement	Intercrystalline	Tidal flat
FM3	Dolo-mudstone with fenestral fabric	Figure 3c	Fenestral fabric, fine to medium grained xenotopic to hypidiotopic dolomite crystal	Dolomitization, fenestral fabric and dissolution	-	Tidal flat
FM4	Stromatolite boundstone	Figure 3d	Massive, thiny lamination	-	-	Tidal flat
FM5	Thrombolite boundstone	Figure 3e	Massive, ostracods, foraminifera and pelloids	Cementation and micritization	-	Tidal flat
FM6	Peloidal intraclastic packstone	Figure 3f	Massive, grain grading and orientation, peloids and intraclasts and bioclast fragments	Dolomitization and cementation and pore filling anhydrite cement	Interparticle and intraparticle	Tidal flat
FM7	Mudstone	Figure 3g	Massive, bioturbation and small bioclast	Bioturbation	Intercrystalline	Lagoon
FM8	Bioclastic wackestone	Figure 3h	Micrite envelope and bioturbation, benthic foraminifera, miliolida, gastropoda and peloid	Bioturbation, stylolitization and micritization	Interparticle and intraparticle	Lagoon
FM9	Peloidal bioclastic packstone	Figure 3i	Micrite envelope and bioturbation, benthic foraminifera, green algae, miliolida, gastropoda and peloid	Micritization, bioturbation and dissolution	Intraparticle and intercrystalline	Lagoon
FM10	Ooid-bioclastic grainstone	Figure 3j	Micrite envelope, cross bedding and orientation, ooid, bioclast particles and benthic foraminifera	Dolomitization, cementation, dissolution, stylolitization, anhydrite cement and fracturing	Interparticle, intraparticle and moldic	Shoal
FM11	Ooid grainstone	Figure 3k	Micrite envelope, cross bedding and orientation, medium-sized and well sorted ooids	Cementation, dolomitization, dissolution, compaction and Anhydrite cement	Interparticle, intraparticle, intercrystalline and moldic	Shoal
FM12	Bioclastic intraclast grainstone	Figure 3l	Cross bedding grain grading and orientation, bioclasts, intraclasts, ooids and benthic foraminifera	Cementation, dissolution, compaction and anhydrite cement	Interparticle, intraparticle, crystalline and vuggy	Shoal
FM13	Bioclastic intraclastic packstone	Figure 3m	Micrite envelope, intraclasts, benthic foraminifera and bivalve fragments	Dissolution, dolomitization, micritization, compaction and fracturing	Intercrystalline and intraparticle	Open marine
FM14	Bioclastic wackestone	Figure 3n	Micrite envelope, Pelagic fauna, sponge spicular, bivalve fragments	Dolomitization, stylolitization, fracturing and micritization	interparticle	Open marine
FM15	Mudstone	Figure 3o	Massive, bioclasts fragments and pelagic fauna	Dolomitization and stylolitization	-	Open marine

B is equal to 1% (Fig. 4). It lacks fossil traces, bioturbation, and diagenetic processes. This microfacies was observed at the top of the K1, K2, and K4 reservoir units in association with dolomitic mudstone microfacies (MF2) (Fig. 8).

4.1.1.2. Dolo-mudstone with anhydrite nodules (MF2)

This microfacies includes dolomitic mudstone with scattered anhydrite nodules, radially parallel to semi-parallel and chicken-wire texture. Dolomite crystals are smaller than 20 microns and are xenotopic (anhedral) to hypidiotopic (subhedral) (Fig. 3 (b)). The abundance of this microfacies in wells A and B is equal to 2 and 3%, respectively (Fig. 4). This microfacies lacks observable biological effects and is observed in association with MF1 and MF2 at the base of K1 and K4 reservoir units (Fig. 8).

4.1.1.3. Dolo-mudstone with fenestral fabric (MF3)

This microfacies is fine-grained dolomitic mudstone, with fenestral fabric and lack of traces of marine organisms. It has been deposited in the low-energy conditions of the tidal flat (Shinn, 1983; Adabi, 2009; Moeini et al., 2023). The abundance of this microfacies in wells A and B is equal to 3 and 4%, respectively (Fig. 4). The pore spaces have been dominantly filled by anhydrite and calcite cements (Fig. 3c). Dolomites were formed during early diagenesis and their size is less than 20 microns, xenotopic to hypidiotopic. Biological effects have not been observed. This microfacies is interlayered with MF1 and MF2 at the base of K1-K4 and the top of K3 reservoir units (Fig. 8).

4.1.1.4. Stromatolite boundstone (MF4)

This microfacies is composed of alternating fine dark and light layers with algal fragments and bioturbation (Fig. 3 (d)). The abundance of this microfacies in wells A and B is equal to 1% (Fig. 4). Its various types are seen

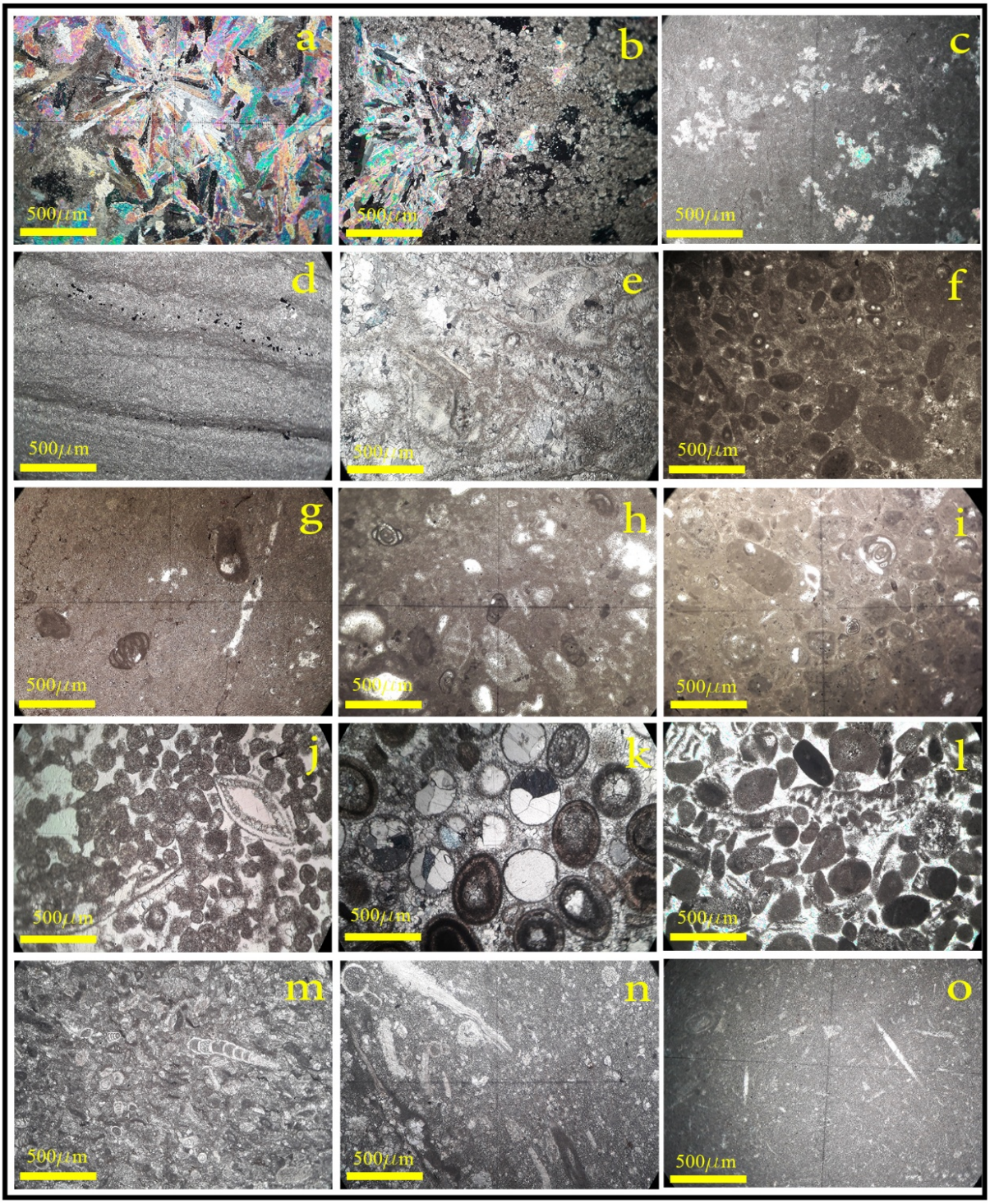

Figure 3. Photomicrographs of microfacies under plane-polarized light (PPL) and cross-polarized light (XPL): (a) layered to nodular anhydrite, (MF1) (XPL) (b) Dolo-mudstone with anhydrite nodules, (MF2) (XPL) (c) dolomudstone with fenestral fabric, (MF3) (PPL) (d) stromatolite boundstone, (MF4) (PPL) (e) thrombolite boundstone, (MF5) (PPL) (f) peloidal intraclastic packstone, (MF6) (PPL) (g) mudstone, (MF7) (PPL) (h) bioclastic wackestone, (MF8) (PPL) (i) peloidal bioclastic packstone, (MF9) (PPL), (j) ooid-bioclastic grainstone, (MF10) (PPL) (k) ooid grainstone, (MF11) (PPL) (l) bioclastic intraclast grainstone, (MF12) (PPL) (m) bioclastic intraclast packstone, (MF13) (PPL) (n) bioclastic wackestone, (MF14) (PPL) (o) mudstone, (MF15) (PPL).

at the scale of several millimeters along with MF2 and MF3 with evaporite nodules and fenestral fabric filled with calcite and anhydrite cements. This facies is widely observed in K2 and K4 reservoir units (Fig. 8).

4.1.1.5. Thrombolite boundstone (MF5)

This microfacies is characterized by massive to clotted fabric and accumulation of microbial, bacterial, and algal microcolonies along with bivalve and ostracod fragments (Fig. 3 (e)). The abundance of this microfacies in studied wells is less than 1% (Fig. 4). This microfacies was observed in the lower part of the Kangan Formation above the boundary of the Permian-Triassic at the base of the K2

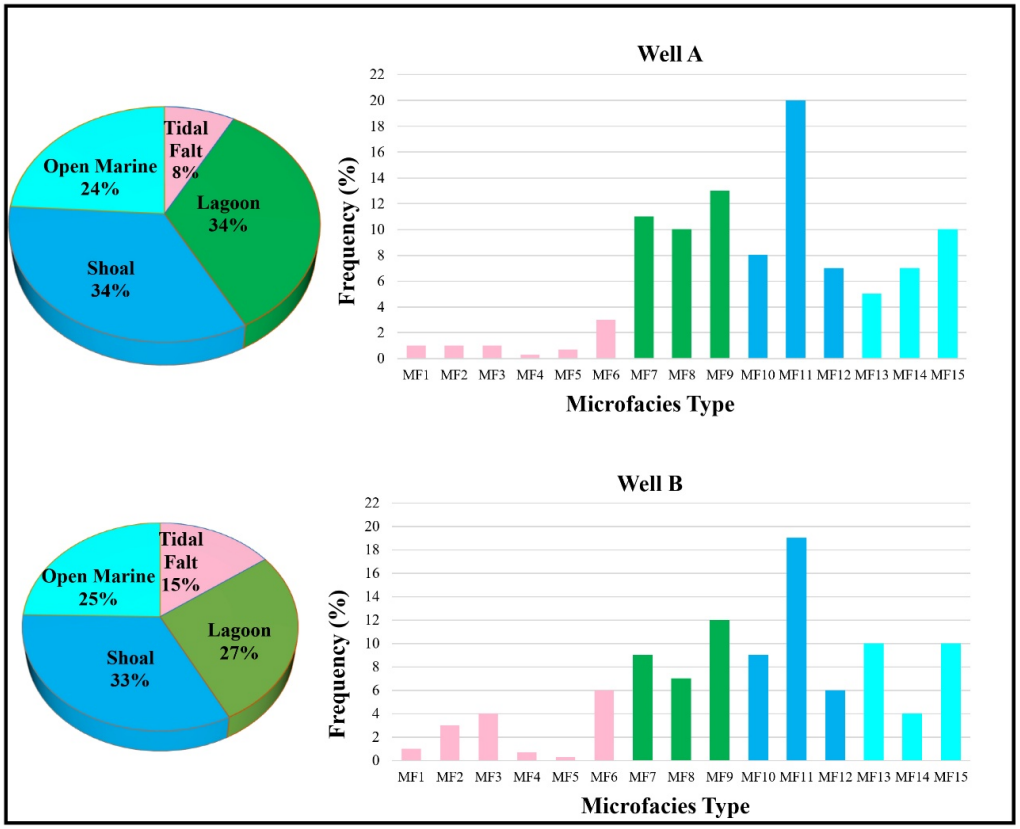

Figure 4. Frequency of microfacies and environments of the studied fields.

reservoir zone (Fig. 8).

4.1.1.6. Peloidal intraclastic packstone (MF6)

Intraclasts with poor sorting are less than 150 microns and angular. They comprise approximately 30% of the constituents (Fig. 3 (f)). Peloids with diameters of less than 150 microns comprise about 20% of allochems of this microfacies and were probably formed due to the breaking and erosion of intraclasts. Small amounts of bivalve fragments and green algae are also observed. The abundance of these microfacies in wells A and B is equal to 4 and 6%, respectively (Fig. 4). Part of the matrix and allochems are dolomitic. The pore spaces between allochems have been filled with anhydrite and calcite cements. The mentioned deposits were observed in the lower part of K1-K4 reservoir units (Fig. 8).

Interpretation: The combination of anhydritic dolomudstones with fenestral fabric, stromatolite boundstones, and layered to nodular anhydrites indicates deposition in the tidal flat environment. In hot and dry climates, due to the high rate of evaporation and the formation of sulfate-rich brines, anhydrites were deposited with different textures such as layered and nodular in the upper part of the tidal flat (Sarg, 1988; Warren, 2006; Lucia, 2007). Gradually, with increasing salinity, the number and size of these nodules are increased and they form a chicken-wire texture (Prothero et al., 1996; Warren, 2006). The fenestral fabric is formed by the decomposition of organic materials and the creation of gas bubbles and their release at the same time as sedimentation in the middle to upper parts of the depositional zone in calcareous facies (Flugel, 2020). Stromatolites are formed as a result of microbial activities and sediment trapping by cyanobacteria in the upper part of the intertidal zone (Flugel, 2020). This facies association is the least common in the studied wells, accounting for 12% and 15% respectively (Fig. 4).

4.1.2 Lagoon facies association

This facies association includes mudstone, bioclastic wackestone, and peloidal bioclastic packstone.

4.1.2.1. Mudstone (MF7)

This microfacies has small amounts of bioclasts, such as miliolida, gastropoda, and shell fragments floating in a micrite and microspar matrix (Fig. 3 (g)). Micrites are often dolomitized and sometimes being affected by neomorphism in the form of microspars is observed. The microfacies abundance in wells A and B corresponds to 11% and 9%, respectively (Fig. 4). The presence of bioturbation indicates limited water circulation and low environmental energy at the time of deposition. This microfacies is observed both at the lowermost and uppermost sections of the reservoir units. Its association with the mudstones of the tidal flat indicates the transition from the tidal flat to the lagoon (Read, 1985; Khalifa, 2005; Insalaco et al., 2006).

4.1.2.2. Bioclastic wackestone (MF8)

This microfacies includes lagoonal bioclasts such as miliolida, gastropoda, bivalve fragments, green algae, and benthic foraminifera accounting for $20-30\%$, which were deposited in a micritic setting (Fig. 3 (h)). Peloids are less common (average 5%). The microfacies abundance in wells A and B are 10% and 7%, respectively (Fig. 4). The fea-

tures of this facies include micritization, stylolitization, and bioturbation. The pore types are interparticle and intraparticle which are often blocked by calcite and anhydrite cements. This facies has been observed alternating with lagoonal mudstones at the bottom and top of the reservoir units (Fig. 8).

4.1.2.3. Peloidal bioclastic packstone (MF9)

Different types of lagoonal bioclasts are present, including miliolida, gastropods, and green algae, with a frequency greater than 30%, as well as peloid and oncoid allochems, which occur at frequencies between 15 – 20%. The abundance of this microfacies in wells A and B is equal to 13 and 12%, respectively (Fig. 4). Regarding its connection to the open marine, this environment displays greater biodiversity, as evidenced by the increased prevalence of protected lagoon allochems (Fig. 3 (i)). Micritization and bioturbation are the main characteristics of this microfacies. Intraparticle and intercrystalline pores are observed. In the studied wells, it was observed at the top of the K1 and K4 reservoir units (Fig. 8).

Interpretation: The mud-supported texture, together with the presence of bioclasts of gastropoda, miliolida, green calcareous algae, peloids, and also the development of micritization and biological disturbances indicate the deposition in the lagoonal environment (Tucker and Wright, 1990; Flugel, 2020). Abundant micrite indicates the low energy of the environment and limited water circulation (Tomasovych, 2004; Flugel, 2020). Considering the presence of green calcareous algae and peloids, this microfacies is attributed to low energy lagoonal environment. Today, peloidal microfacies are being formed in the middle part of the Bahama Plateau and the southern shores of the Persian Gulf in the lagoon environment (Tucker and Wright, 1990; Burchette and Wright, 1992). Green algae are abundant in the area of light penetration, in calm conditions of environmental energy and at a depth of about 3 to 5 meters. The warm waters of shallow protected lagoons are a suitable place for these organisms to live (Tucker and Wright, 1990; Reading, 1996). The abundance of mud- and grain-supported microfacies in the lagoon environment, in wells A and B, is equal to 34 and 27%, respectively (Fig. 4).

4.1.3 Shoal facies association

This facies association includes ooid-bioclastic grainstone, ooid grainstone, and bioclastic intraclastic grainstone.

4.1.3.1. Ooid-bioclastic grainstone (MF10)

The most important constituents of this microfacies are micritized ooids, with a frequency of about 30% and often smaller than one millimeter. Bioclasts such as benthic foraminifera, bivalve fragments and gastropoda, intraclasts, and peloids are also present, constituting 10 – 20% of the sample. (Fig. 3 (j)). The abundance of this microfacies in wells A and B is equal to 8 and 9%, respectively (Fig. 4). Micritization, dolomitization, dissolution, and primary marine cementation such as acicular to fibrous isopachous cements and bladed calcite are the most important diagenetic processes. Fractures are seen with less frequency (Rafiei et al., 2016; Kaveh-Ahangar et al., 2023). Dolomites are euhedral and subhedral and smaller than 40 microns. Ooids are often micritic. Intraparticle, interparticle, and moldic pores are observed in this microfacies. Pores have been filled with calcite and anhydrite cements in many cases. This microfacies was observed in K1, K2, and K3 reservoir units of well A and K1 and K3 reservoirs units in well B along with lagoonal facies (Fig. 8).

4.1.3.2. Ooid grainstone (MF11)

This microfacies is composed of 30 – 50% medium-sized (0.5 – 1 mm), well-sorted ooids showing micritization in some cases (Fig. 3 (k)). Along with ooids, fragments of bivalve fossils and benthic foraminifera (5%) are observed. The abundance of these microfacies in studied wells is about 20% (Fig. 4). Dolomitized ooids are observed in several intervals. Good sorting and maturity along with primary marine cements such as acicular to fibrous isopachous and bladed calcite indicate high-energy and high-water circulation during the formation of this microfacies. Ooid grainstone is one of the dominant microfacies in the studied sequences. Dolomitization, dissolution, cementation, and mechanical compaction are diagenetic processes that have affected this facies (Fig. 6). Dissolution led to the formation of extensive moldic and intraparticle pores. In some cases, these pores have been filled with anhydrite and calcite cements.

4.1.3.3. Bioclastic intraclast grainstone (MF12)

This microfacies with grain-supported texture includes 30%

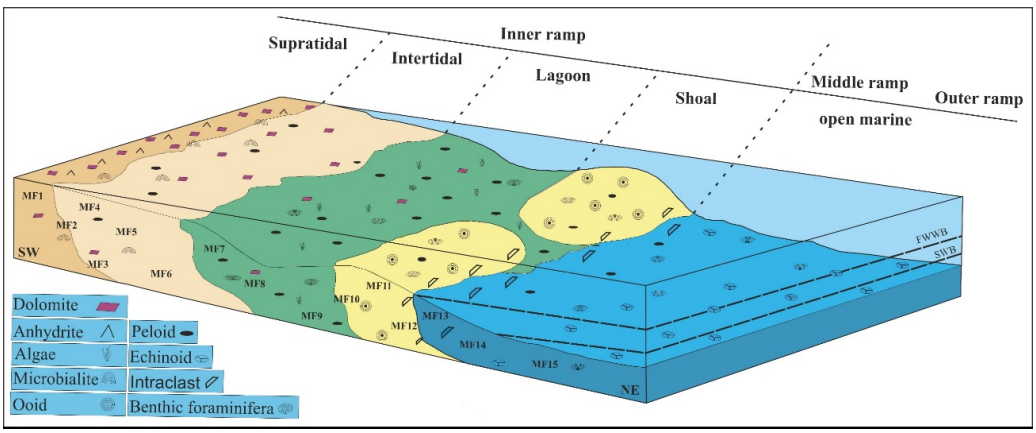

Figure 5. Depositional model of the Upper Dalan Member and the Kangan Formation in the studied fields.

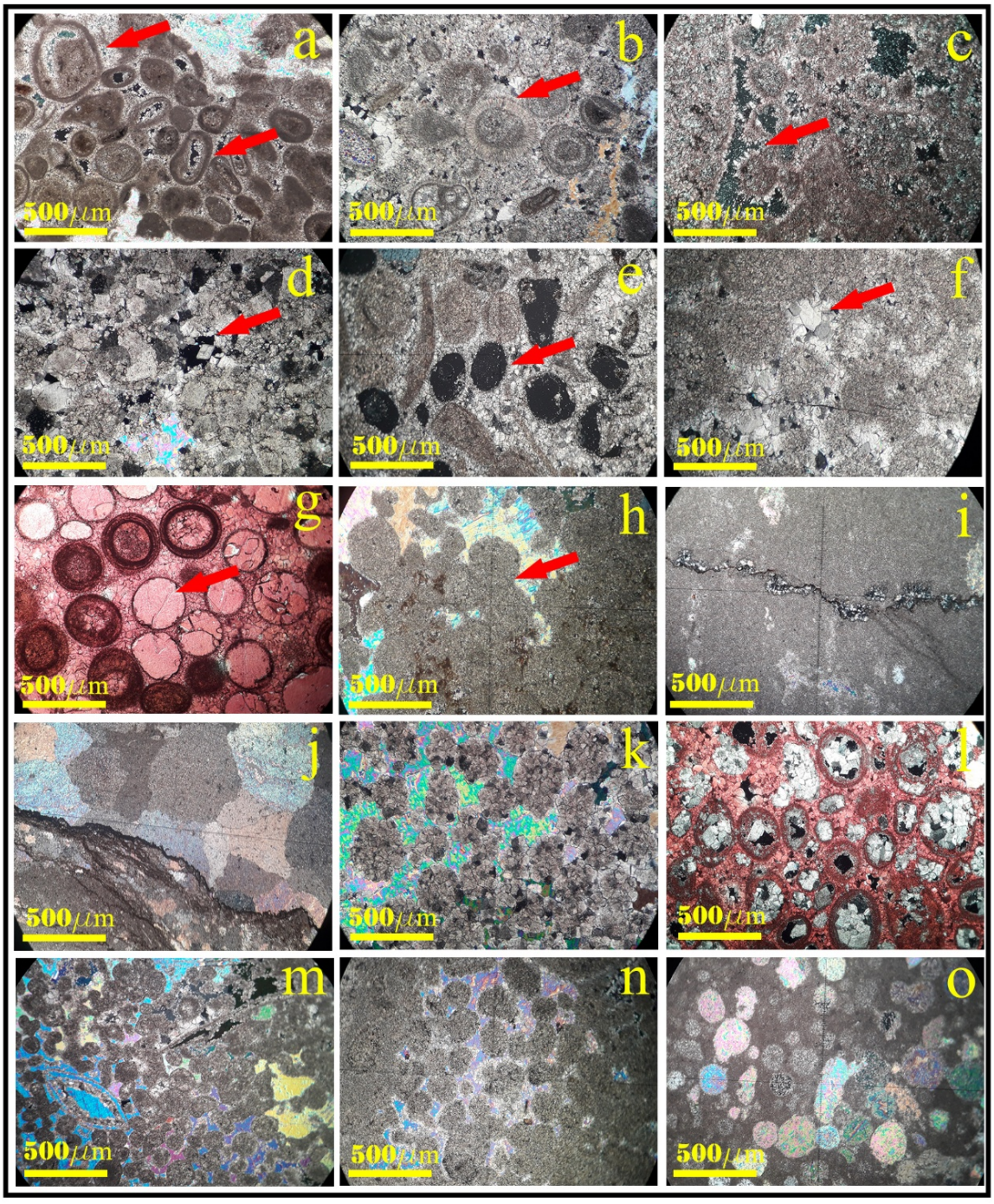

Figure 6. Photomicrographs of the main diagenetic processes of the Upper Dalan Member and the Kangan Formation: (a) micritization around the allochems, some grains have been dissolved and show a micritic coating (arrows) (XPL), (b) acicular to fibrous isopachous cement, formed in the marine environment (XPL), (c) bladed calcite cement around the ooid grains in the facies of the high-energy diagenetic environment (XPL), (d) dolomitization of the mudstone facies along with nodular anhydrite in the tidal flat, intercrystalline pores are observed in the facies (arrow) (XPL), (e) selective dissolution in the ooid grainstone facies and creation of moldic pores (XPL), (f) drusy cement in the ooid grainstone facies has been expanded in the meteoric environment, (g) blocky cement filling the moldic porosity in the ooid grainstone facies (XPL), (h) expansion of the folded and concave-convex texture in between grains in the burial diagenetic environment (XPL), (i) stylolitization in the burial diagenetic environment and the formation of fine crystal dolomite after the process of chemical condensation in the burial diagenetic environment (XPL), (j) the formation of solution seam during the burial diagenesis (XPL), (k) selective dolomitization in the ooid grainstone facies during the burial diagenesis (XPL), (l) dolomite cement filling moldic pores, coarse crystal and rhombohedral dolomites are formed in the pore inside ooid grains (arrow) (XPL), (m) pervasive anhydrite cement in the ooid-bioclast grainstone facies during the burial diagenesis (XPL), (n) poikilotopic cement anhydrite, (o) anhydrite cement filling moldic pores caused by selective dissolution (XPL).

coarse angular intraclasts and various bioclasts such as echinoderms, benthic foraminifera, and bivalve fragments by 10 – 20% frequency. Ooids and peloids (up to 5%) have also been observed (Fig. 3 (l)). The abundance of this microfacies in wells A and B is equal to 7 and 6%, respectively (Fig. 4). The mentioned microfacies has been observed in selected wells along with the packstone facies of the open marine environment. Cementation, dissolution, dolomitization, and physical compaction are the dominant diagenetic processes (Fig. 6). Marine cements of equant calcite, acicular to fibrous isopachous cements and bladed calcites are the most frequent types of cements. Interparticle, vuggy, intercrystalline and intraparticle pores are also observed in this microfacies.

Interpretation: The presence of ooids with grain-supported texture, high textural maturity, and primary marine cements in this microfacies indicate their deposition in a high-energy environment with high water circulation (Wilson, 1975). The presence of a significant proportion of ooids, coupled with the occurrence of bioclasts (including bivalves and benthic foraminifera), peloids, and intraclasts, implies that the depositional environment was characterized by high-energy conditions. Ooids are formed at a very shallow depth (diameters less than 2 meters) in marine environments with high salinity and supersaturated with calcium carbonate in shoals (Tucker, 2001; Flugel, 2020). The grainstone facies of the shoal have the greatest thickness in the studied sequence with a frequency of about 33% in both wells (Fig. 4). Ooid grainstone is the most common microfacies and suggests that high and stable energy conditions prevailed during its formation.

4.1.4 Open marine facies association

This facies association includes intraclastic bioclastic packstone, bioclastic wackestone and mudstone.

4.1.4.1. Bioclastic intraclastic packstone (MF13)

This microfacies includes intraclast fragments (about 25%, ranging from 0.2 to 0.5 mm), benthic foraminifera, crinoid and bivalve fragments (around 15%) (Fig. 3 (m)). This microfacies has been observed in wells A and B with 5 and 10% frequency, respectively (Fig. 4). The microfacies of MF13 exhibits greater thickness in units K2 and K3 of Well A, as well as units K1 and K3 of Well B, compared to other units within these wells (Fig. 8). Diagenetic processes of dissolution, micritization, fracturing, dolomitization and physical compaction have been observed in this microfacies (Fig. 6). Limited porosity has been identified as intercrystalline and intraparticle.

4.1.4.2. Bioclastic wackestone (MF14)

The main constituents of this microfacies include pelagic

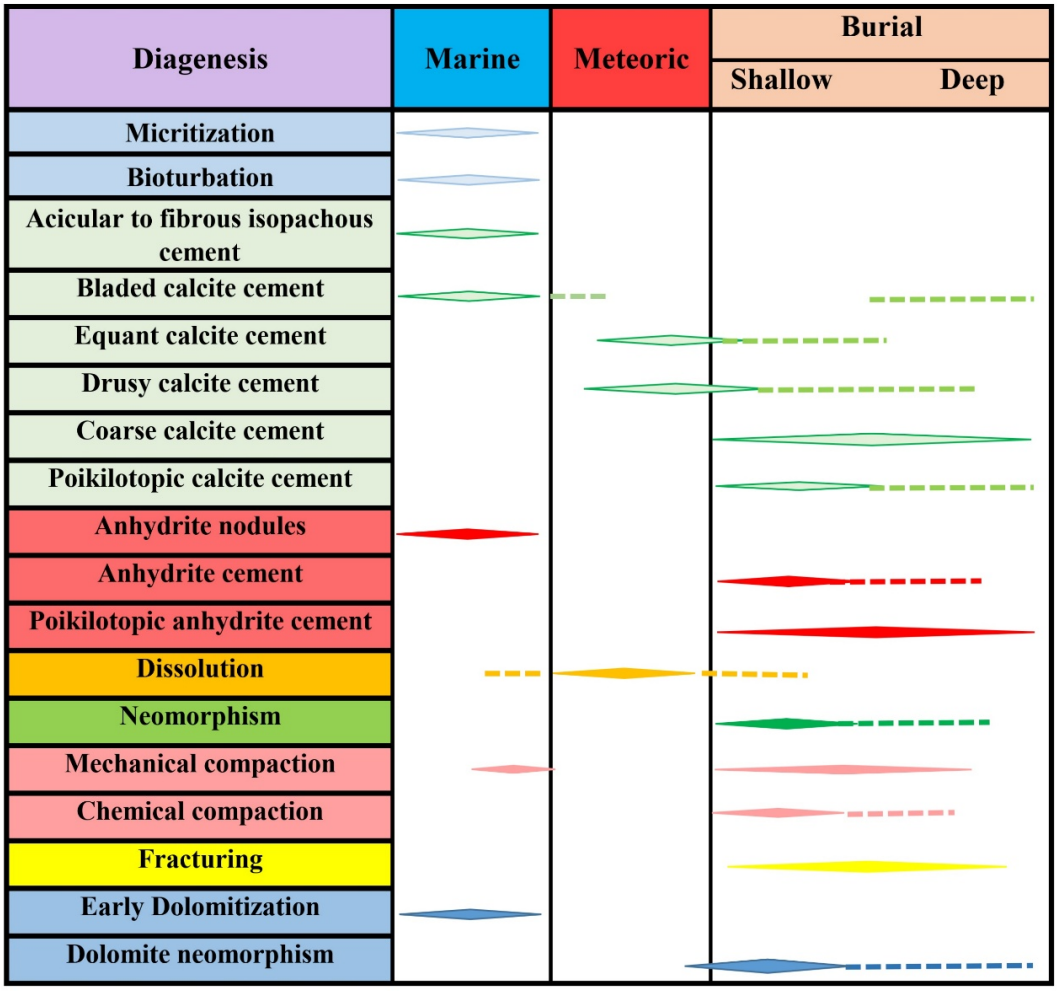

Figure 7. Proposed diagenetic sequence of events in the Upper Dalan member and the Kangan Formation.

fauna, sponge spicules, echinoderm fragments and thin shell bivalve fragments. This microfacies is composed of $10-15\%$ floating bioclast fragments in a micritic matrix (Fig. 3 (n)). The abundance of these microfacies in wells A and B is equal to 7 and 4%, respectively (Fig. 4). Micritization, stylolitization, fracturing and dolomitization are the diagenetic features which were observed in this microfacies. In Well A, the K3 unit is characterized by a significant thickness, which is observed as an interlayer with the mudstones of the outer ramp environment. In contrast, the K1 and K2 units exhibit a small thickness compared to the K3 unit. In well B, it has been observed in K1, K3 and K4 units with low thickness and abundant pelagic fauna (Fig. 8).

4.1.4.3. Mudstone (MF15)

This microfacies has a micritic matrix and contains less than 5% of bioclast fragments consisting of thin bivalve shells, echinoderm fragments, pelagic fauna, and sponge spicules (Fig. 3 (o)). The abundance of these microfacies in studied wells is less than 10% (Fig. 4). Dolomites of different sizes and smaller than 30 microns were observed, displaying subhedral and euhedral forms. The micritic matrix represents the sedimentation of this microfacies in a low-energy environment. Dolomitization and stylolitization are seen in several intervals. The microfacies of MF15 has more thickness in the unit of K1 in comparison with other units (Fig. 8). In well B, it was deposited in K4 reservoir unit with a large thickness along with wackestone deposits of the open marine facies association. In the remaining reservoir units, the thickness is relatively low (Fig. 8).

Interpretation: The abundance of pelagic fauna, sponge spicules, and echinoderm fragments, along with thin shell bivalve fragments in a mud-supported texture indicates a low-energy open marine environment and below the base of normal waves (Tucker, 2001; Flugel, 2020). Sponges are observed in anaerobic conditions in the deeper parts of the open marine along with other pelagic fauna. Due to the presence of large-sized intraclasts and bioclasts, packstone microfacies indicate deposition in a high-energy environment, above the storm wave base in the middle ramp (Insalaco et al., 2006). The abundance of the open marine samples is equivalent to 21% and 25% for wells A and B, respectively (Fig. 4).

4.2 Depositional setting

Microfacies frequency, and type of skeletal and non-skeletal components indicate their deposition in a shallow carbonate platform. Based on the lateral changes of the facies, texture, and their abundance, four facies associations including tidal flat, lagoon, shoal, and open marine were identified. The extensive lateral continuity of carbonate-evaporite sequences suggests that the Permian–Triassic strata have been deposited in a carbonate ramp environment (Al-ali et al., 2013; Amel et al., 2015; Karimi et al., 2015; Jafarian et al., 2017). The lack of reef facies and the remnants of reef-building organisms (Read, 1985) and, high frequency of ooid and bioclastic grainstone microfacies, are in agreement with this interpretation (Kakemem et al., 2021; Kakemem et al., 2023). The genetic classification of the homoclinal carbonate ramp by Burchette and Wright (1992) exhibits similar characteristics to those found in this study.

4.3 Diagenesis

Based on petrography studies, micritization, cementation, dissolution, compaction, and dolomitization have been identified in the Upper Dalan Member and the Kangan Formation in the studied wells. These processes have occurred in marine, meteoric, and deep burial diagenetic environments.

4.3.1 Marine diagenesis

The main diagenetic processes in marine environments include micritization and marine cementation. Micritization was observed in grainstone and packstone microfacies, on skeletal and non-skeletal allochems in the Upper Dalan Member and the Kangan Formation. Due to the activity of microbial organisms, a thin and dark micritic cover was formed around the ooids and skeletal grains (Fig. 6 (a)). Early marine cements have been formed, including acicular to fibrous isopachous cements and bladed calcite around skeletal and non-skeletal grains in the shoal grain-supported facies (Moore, 2001). These types of cements are more frequent in the central and seaward parts of the grainstone microfacies of the Upper Dalan Member and Kangan Formation, around ooids and bioclasts (Figs. 6 (b) and 6 (c)). The interparticle pore spaces have been filled with equant calcite cements. Dolomitization has occurred in mudstone and wackestone microfacies under the influence of evaporation (Fontana et al., 2012). These dolomites are microcrystalline (less than 30 μm), xenotopic to hypidiotopic, and are observed along with scattered nodules of anhydrite (Fig. 6 (d)). Alsharhan (2006) believes that the dolomitized mudstones of the tidal flat along with anhydrite nodules were formed in an early diagenetic environment. Lucia (2007), explains the formation of this type of anhydrite nodules in the early stages of syn-depositional diagenesis or shortly after sedimentation as a result of increasing salinity, creating supersaturated sulfate solutions.

4.3.2 Meteoric diagenesis

Meteoric diagenesis has affected the Upper Dalan Member and the Kangan Formation during the sea-level fall and subaerial exposure of sediments (Tavakoli, 2015). Due to this process, sediments have been dissolved, and moldic and vuggy porosities have been created. Selective dissolution in allochems such as ooids and bioclasts has caused the creation of moldic pores in the depositional succession (Fig. 6 (e)).

Davoodi et al. (2024) believed that two types of dissolution have occurred due to meteoric and burial diagenesis in the studied sequences. According to this study, meteoric dissolution occurred in the shallow meteoric realm while sediments were not completely lithified. Cements related to the meteoric diagenetic environment, such as drusy and blocky, were precipitated in inter and intra-particle pores (Figs. 6 (f) and 6 (g)). Both processes of meteoric cementation and dissolution were observed at the top of the Upper Dalan Member, which indicates the influence of meteoric diagenesis after the exposure.

4.3.3 Deep burial diagenesis

The burial diagenetic environment is characterized by mechanical and chemical compaction, cementation, and dissolution. Mechanical compaction has caused a decrease in the thickness of the sediments, a change in the shape of the grains, and the creation of concave and convex-concave contacts between the grains. It is more common in ooids of grainstone facies (Fig. 6 (h)). Chemical compaction was observed as an important diagenetic process in the deep burial zone, in the form of stylolitization and formation of solution seams. This process is an important source for burial cements due to the dissolution of grains and matrix (Hosseinzadeh and Tavakoli, 2024).

In the studied intervals, sharp and wavy stylolites are often observed in the grain-supported facies with both large and small amplitudes. Stylolites with small amplitude usually contain microcrystalline and rhombohedral dolomites (Figs. 6 (i) and 6 (j)). These dolomites are likely linked to deep burial diagenesis, as they formed subsequent to the stylolitization process. Dolomitization occurred through a fabric-selective replacement process. The dolomites are characterized by coarse grain sizes and exhibit subhedral to euhedral textures, which have replaced ooids and bioclasts within the grainstone microfacies. Dolomite cements have been observed filling moldic pores in both the Upper Dalan Member and the Kangan Formation. These cements are characterized by coarse, rhombohedral crystals, which formed under deep burial diagenetic conditions (Figs. 6 (k) and 6 (l)).

Anhydrite cements were formed in poikilotopic and pore-filling forms during the burial diagenetic stage. Petrographic evidence, such as coarse crystals, filling of interparticle and

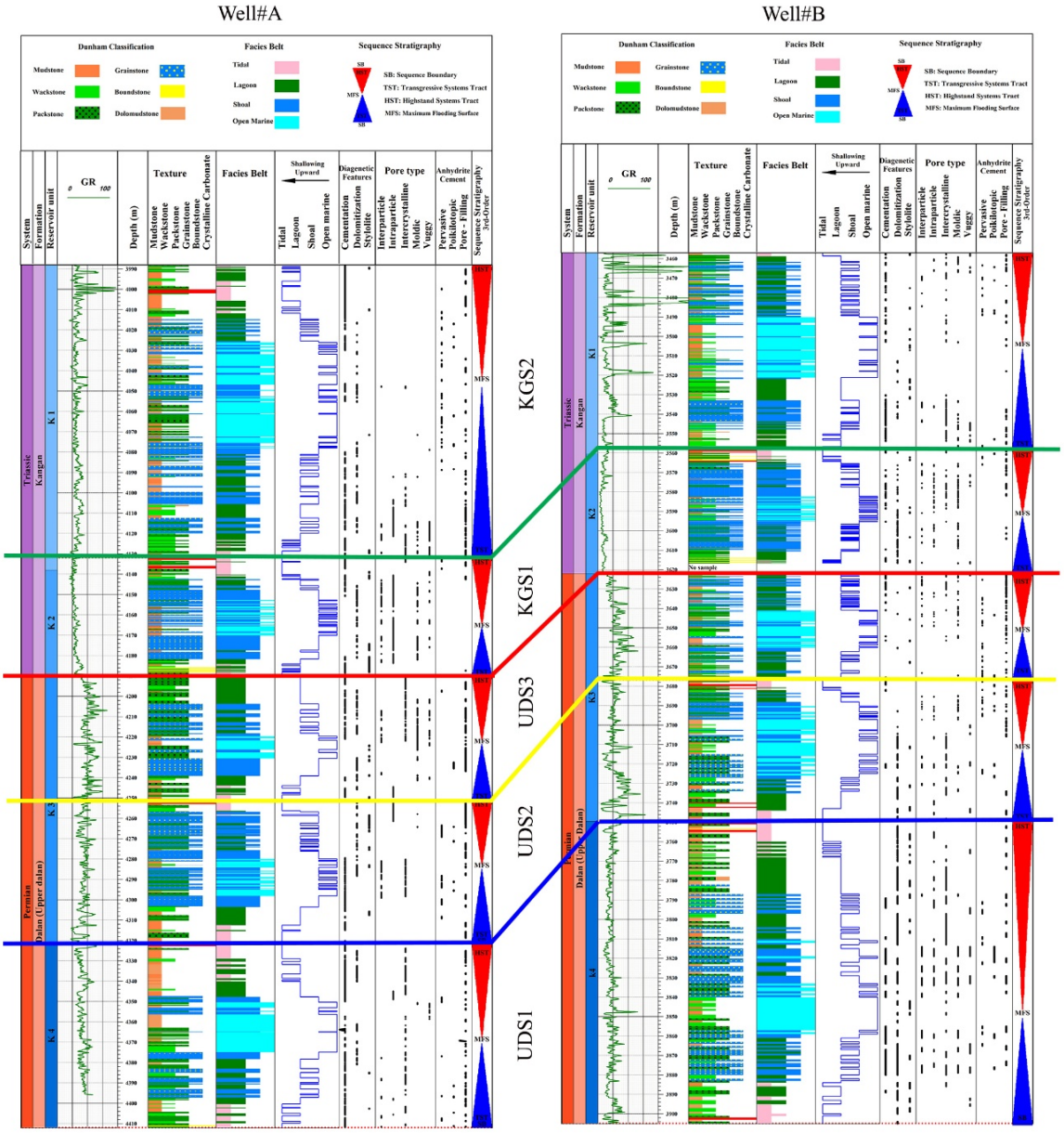

Figure 8. Stratigraphic column including textural and environmental features, microfacies and sequence stratigraphy of the studied wells.

moldic pores, and fractures, indicate the formation of these anhydrite cements in a deep burial environment (Figs. 6 (n), 6 (m), and 6 (o)). The diagenetic sequence of the studied formations and the relative time of their formation are shown in figure 7.

4.4 Sequence stratigraphy

The study of microfacies, their lateral and vertical changes, and comparison with gamma-ray data have allowed the identification of five 3rd order depositional sequences in the Upper Dalan Member and the Kangan Formation.

4.4.1 Upper Dalan depositional sequence 1 (UDS1)

From bottom to top, the first sequence has a thickness of 155 meters in well A and 92 meters in well B. Its lower boundary is marked by an unconformity and is defined by the evaporite Nar Member (Szabo and Kheradpir, 1978) (Fig. 2). This sequence begins with packstone grain-supported facies and continues with dolo-mudstones of the tidal flat facies association. Its TST includes mud-supported to grain-supported facies that were deposited in tidal flat to open marine environments with a deepening upward trend. Due to an increase in the accommodation space, some mudstone microfacies containing pelagic fauna and sponge spicules were also deposited (Fig. 8), which were interpreted as the MFS and can be correlated with gamma-ray signatures (Tavakoli, 2017).

With the reduction of the accommodation space, mudstone and bioclastic wackestone facies of the open marine environment were deposited. Subsequently, as the accommodation space decreased, grainstones, indicative of a shoal setting, were identified indicating a high-energy environment. Dolomudstones, stromatolitic boundstones, and anhydrite facies were deposited at the top of the HST. This sequence is equivalent to KS4 of Alsharhan (2006) and Cycle IV of Insalaco et al. (2006).

The lowest depositional sequence in well A is thicker than well B. Furthermore, the grainstone facies within the shoal environment of this well exhibits a greater thickness, indicating the prevalence of high energy conditions during the deposition of this sedimentary interval (Fig. 8).

4.4.2 Upper Dalan depositional sequence 2 (UDS2)

The lagoonal facies and the grainstones of the shoal setting comprise the greatest thickness of the TST of this depositional sequence. The upward deepening trend in this systems tract continues with mud-supported facies of open marine and terminates with mudstone facies. The MFS in this depositional sequence is characterized by mudstone facies containing pelagic fauna and sponge spicules of the outer ramp and an increase in the gamma-ray signal. The HST was determined based on sedimentological observations, fossil evidence, and gamma-ray data, with a prograding and shallowing upward succession including open-marine, shoal, and lagoonal deposits, respectively (Fig. 8). This systems tract mainly includes grain-supported microfacies of ooid and bioclastic grainstone related to the shoal and indicates low depth and high energy with an aggradational staking pattern at the time of deposition. The thickness of this sequence in both wells is about 70 meters and is equivalent to KS3 Alsharhan (2006) and cycle III of Insalaco et al. (2006).

4.4.3 Upper Dalan depositional sequence 3 (UDS3)

The third depositional sequence was deposited with almost the same thickness in the studied fields (well A: 54 m and well B: 62 m). The TST in this depositional sequence begins with mudstone microfacies along with tidal flat evaporites and peloidal intraclastic packstones. Then, coeval with the rise of the relative sea level, mud-supporting facies of the lagoon (MF7, Mf8, and MF9) were deposited. This sequence continues with the presence of ooid-bioclastic grainstone and intraclastic facies of the shoal setting and is finally covered by bioclastic wackestone and mudstone deposits along with bioclastic intraclastic packstones. The mudstones of the open marine facies association correspond to the maximum flooding surface, as they are the highest bathymetric deposits recognized in the sequence. This surface has been determined based on sedimentological evidence and the maximum increase of the gamma-ray signal. At the end of sea-level rise and subsequent reduction in accommodation space, the HST has been identified, comprising open marine, shoal, and lagoon facies associations. These facies were deposited in the outer, middle, and inner ramp showing a progressive and shallowing upward trend, respectively. The grain-supported facies of ooid and bioclastic grainstone with interlayers of lagoonal wackestone form the thickest interval. The microfacies of the tidal flat have not been observed in this systems tract, which is probably due to the subaerial exposure and erosion of the mentioned sediments. The upper boundary of this sequence is a subaerial unconformity, corresponding to the PTB (Sharland et al., 2001; Tavakoli et al., 2018; Tavakoli and Hassani, 2022; Kakemem et al., 2023). This sequence is equivalent to KS2 of Alsharhan (2006) and the 4th sequence (KS3b) of Insalaco et al. (2006).

4.4.4 Kangan depositional sequence 1 (KGS1)

The thickness of this depositional sequence in well A is 64 meters and in well B is 58 meters. The sequence begins with tidal flat facies (MF1, MF2, and MF3) and thrombolite facies (MF4). With the rise in the relative sea level, the succession was overlain by mud-supported and grain-supported lagoon deposits (MF6, MF7, and MF8). The ooid and bioclastic grainstone facies of the shoal setting were deposited in TST with a significant thickness. With the continuation of the relative sea level rise, the open marine facies associations (MF13, MF14, and MF15) were deposited overlaying the shoal microfacies. The maximum rise of the sea level in this sequence is determined by the formation of a thin layer of mudstone microfacies of the outer ramp and the increase in the gamma-ray signal. This microfacies includes thin-shell bivalve and pelagic fauna, and traces of sponge spicules (Fig. 8).

The topmost systems tract begins with mud-supported microfacies (MF14, MF15) of the open marine facies association and then is covered by grain-supported microfacies (MF10, MF11 and MF12) of the shoal facies association. The grainstones within the shoal setting represent energetic and shallow marine facies, and were deposited during the

HST with an aggradational stacking pattern. This progressive succession continues with mudstone and bioclastic wackestone (MF7 and MF8) of the lagoon facies association and terminates with peloidal intraclastic packstone, dolo-mudstone with fenestral fabric and layered to nodular anhydrite (MF6, MF3 and MF1) of the tidal flat facies association. This depositional sequence is partly equivalent to the cycle II of Insalaco et al. (2006).

4.4.5 Kangan depositional sequence 2 (KGS2)

The thickness of the second depositional sequence of the Kangan Formation in wells A and B, is 102 and 144 meters, respectively (Fig. 8). The TST deposits begins with peloidal intraclastic grain-supported facies and mud-supported dolomudstone facies (MF7, MF3 and MF2). Due to the rapid increase in the relative sea-level and creation of the accommodation space, the sequence continues with the lagoonal facies (MF7, MF8 and MF9). Subsequently, grain-supported shoal microfacies (MF10 and MF11) were deposited on top of them. The middle ramp mud-dominated microfacies, bioclastic wackestone and mudstone were deposited at the top of this sequence, showing a deepening upward trend. The MFS in this sequence is interpreted by a thin layer of mudstone containing echinoderms, showing an increase in the gamma-ray signal. The HST begins with the presence of bioclastic wackestone and bioclastic intraclastic packstone of the open marine facies association, which is overlain by the grainstone microfacies of the shoal facies association (MF10, MF11). The lagoon facies association, characterized by mudstone, bioclastic wackestone, and peloidal bioclastic packstone microfacies, overlies the shoal facies association, illustrating a progressive sequence of depositional environments. At the end of this systems tract, the microfacies of the tidal flat facies association, including intraclastic peloidal packstone and dolo-mudstones with fenestral fabric, are observed. This depositional sequence correlates with cycle I of Insalaco et al. (2006).

5. Discussion

At the beginning of the Middle Permian, coinciding with the rifting and separation of the Arabian Plate from the central Iran Block and the Sanandaj-Sirjan zone, a carbonate ramp with a gentle slope was developed on the northeast margin of the Arabian Plate (Sharland et al., 2001; Alsharhan, 2006). This happened in response to rapid subsidence and the onset of a rising sea level. As a result of the increase in relative sea level in the Late Permian and the changes in the physical and chemical conditions of the depositional environment, the carbonate-evaporite sequences of the Upper Dalan Member have been placed on the evaporitic Nar Member. At the beginning of the sea-level rise, dolo-mudstone facies of the tidal flat facies association and lagoonal wackestones were deposited (Alsharhan, 2006; Fontana et al., 2012). Dolomitization in mudstone facies of tidal flat and open marine has increased permeability and improved reservoir quality in these sequences. Dolomitization in field A has increased permeability and improved reservoir quality by creating intercrystalline pores at the top of UDS1 and UDS3. In field B, dolomitization at the top of the UDS1 and the base of the UDS3 has enhanced the reservoir quality. With the continuation of rapid subsidence and the creation of a suitable accommodation space, the shoal microfacies were deposited in a wide area of the carbonate platform. The high thickness of grainstone facies in this formation indicates a high-energy and shallow environment under the influence of waves (Nazemi et al., 2018; Naderi-Khujin et al., 2020; Nazemi et al., 2021; Naderi-Khujin and Tavakoli, 2023). The facies in the upper part of the TST have high initial porosity and high reservoir quality. In field B, the upper facies in the UDS2 and KGS2 have more porosity and better reservoir quality than those of field A. The TST of the UDS3 shows a more suitable reservoir quality in filed B. The secondary intercrystalline pores resulting from dolomitization has increased porosity and permeability and improved reservoir quality (Soleimani and Tavakoli, 2024). The MFS was identified by the presence of the mudstone facies and corroborated with gamma-ray data. With the reduction of the accommodation space due to changes in the relative sea level, the grainstone facies of the shoal setting related to the HST were deposited in a large part of the platform depicting an aggradational stacking pattern. The early HST facies have a skeletal framework and high primary porosity; therefore, they have good reservoir quality. Compared to field A, the early HST in the UDS2 of field B, presents a better reservoir quality. In field A, the early HST comprises mainly grainstone facies and shows a better reservoir quality due to higher porosity and permeability. The late HST facies have lower porosity and permeability due to the reduction of the relative sea level and the sedimentation of calcite and anhydrite cements. The late HST in field A, has a suitable reservoir quality, while it shows poor quality in field B. Changes in the relative sea level in this period were the result of tectonic and climatic events and have caused the formation of three third-order depositional sequences in the upper Dalan Member (Sharland et al., 2001). At the end of the Permian, with the relative sea level fall and exposure of the deposited sequences, a large part of the Permian sediments was eroded and an important discontinuity was formed (Haq and Shutter, 2008; Haq, 2018; Tavakoli et al., 2018; Kakemem et al., 2021). Moldic and vuggy pores, resulting from dissolution processes, along with the presence of drusy and blocky cements, show evidence of the previously mentioned eroded surface at the uppermost layer of the Upper Dalan Member. This surface has also been observed on the top of the Lower Khuff Formation (Tavakoli and Jamaliyan, 2019).

Deposition of peloidal packstone and mudstone facies at the base of the Kangan Formation overlying the erosional facies of the top of the Dalan Formation indicates the transgression began during the earliest Triassic. This transgression developed as a result of the eustatic rise and rapid subsidence of the passive margin of the north-eastern Arabian Plate (Sharland et al., 2001). The thrombolite facies appeared after the Permian–Triassic extinction. This global extinction has been reported in different parts of the world such as southern China, Vietnam, Turkey and Serbia (Garbelli et al., 2016; Ellwood et al., 2017; Huang et al., 2019; Maaleki-Moghadam et al., 2019). With the rapid rise of the

sea level and the creation of a sufficient accommodation space, the lagoonal facies association and grainstones of the shoal facies association (TST) were deposited on the tidal flat facies association with a deepening upwards trend. Due to the extension of the Triassic Sea (Neo-Tethys) and the dominance of the grainstone facies, the reservoir quality of the uppermost interval of the TST (in the KGS2 of A & B wells) is outstanding. Primary marine cements, such as acicular to fibrous isopachous cement and bladed calcite around the skeletal grains, have created a good framework to preserve primary interparticle pores, which was effective in improving reservoir quality. At the end of the rise of the relative sea level (late TST), the MF15 deposited in an open marine facies association. This facies (MF15) in well B comprises mudstone with pelagic fauna, which indicates the greater depth of deposition in this section compared to well A. This implies that the paleo-slope during the Early Triassic was dipping towards the northeast. The proximity to the center of the Neo-Tethys rift during sediment deposition in the southwest part resulted in the deepening of the basin towards field B. This facies were deposited in the outer ramp during the maximum sea level rise. Dolomitization in the latter facies has increased reservoir quality. In field A, the uppermost section of the UKS1 displays favorable reservoir quality, making it a recommended focus for further study as a reservoir zone. Conversely, this portion exhibits lower reservoir quality in field B. The fluctuations in relative sea level during the Early Triassic period mirrored the broader patterns of sea-level changes, both globally and regionally. These variations played a pivotal role in the development of two third-order depositional sequences within the Kangan Formation (Kakemem et al., 2023).

6. conclusion

The present research draws the following conclusions:

- A total of 15 carbonate-evaporite microfacies belonging to tidal flat, lagoon, shoal and open marine environments were identified. The study is conducted on two wells from two fields in the eastern Persian Gulf.
- The Upper Dalan Member and the Kangan Formation were deposited in a carbonate ramp with a gentle slope towards the northeast, in hot and dry climate.
- Calcite and anhydrite cementation and mechanical compaction are among the most important diagenetic processes that have reduced porosity in depositional facies. On the other hand, dissolution and dolomitization have played a constructive role and have increased reservoir quality.
- For the studied intervals, three 3rd order depositional sequences in the Late Permian and two 3rd order depositional sequences in the Early Triassic have been identified which are comparable with the sequence pattern of the Zagros Basin and the Arabian Plate.
- Tectonic movements at the end of the Permian and also the fall of the sea level led to the development of the erosional surface at the top of the Upper Dalan Member, defined as a sequence boundary and corresponds to the boundary of the Permian–Triassic. This boundary can be seen in the Zagros Basin and the Arabian Plate.

Acknowledgments
The authors thank Dr. Mohsen Kalani and Dr. Mehrangiz Naderi-Khujin for providing valuable comments, we are also grateful to the Iranian Offshore Oil Company (IOOC) and Petroleum Engineering and Development Company (PEDEC) for laboratory support and permission to publish this research. We would like to express our gratitude to the two anonymous reviewers for their valuable feedback and contributions to this work.

Authors contributions
Authors have contributed equally in preparing and writing the manuscript.

Availability of data and materials
The data that support the findings of this study are available from the corresponding author, upon reasonable request.

Conflict of interests
The authors declare that they have no known competing financial interests or personal relationships that could have appeared to influence the work reported in this paper.

References

Abdolmaleki J., Tavakoli V. (2016) Anachronistic facies in the early Triassic successions of the Persian Gulf and its palaeoenvironmental reconstruction. *Palaeogeography, Palaeoclimatology, Palaeoecology* 446:213–224. DOI: https://doi.org/10.1016/j.palaeo.2016.01.031.

Adabi M. H. (2009) Multistage dolomitization of Upper Jurassic Mozduran Formation, Kopet-Dagh Basin, N.E. Iran. *Journal of Carbonates and Evaporites* 24:16–32. DOI: https://doi.org/10.1007/bf03228054.

Al-ali M., Rahimpour-Bonab H., Moussavi-Harami R., Jahani D. (2013) Environmental and sequence stratigraphic implications of anhydrite textures: A case from the Lower Triassic of the Central Persian Gulf. *Journal of Asian Earth Sciences* 75:110–125. DOI: https://doi.org/10.1016/j.jseaes.2013.07.017.

Al-Husseini M. I., Koehrer B. (2013) Chrono- and sequence-stratigraphy of the Mid-Permian to Early Triassic Khuff sequences of the Arabian Plate. *GeoArabia* 18 (3): 103–130. DOI: https://doi.org/10.2113/geoarabia1803103.

Alsharhan A. S. (2006) Sedimentological character and hydrocarbon parameters of the middle Permian to early Triassic Khuff formation, United Arab Emirates. *GeoArabia* 11:121–158. DOI: https://doi.org/10.2113/geoarabia1103121.

Amel H., Jafarian A., Husinec A., Koeshidayatullah A., Swennen R. (2015) Microfacies, depositional environment and diagenetic evolution controls on the reservoir quality of the Permian Upper Dalan Formation, Kish Gas Field. *Journal of Marine and Petroleum Geology* 67:57–71. DOI: https://doi.org/10.1016/j.marpetgeo.2015.04.012.

Asadi-Eskandar A., Rahimpour-Bonab S. H. Hejri, Afsari K., Mardani A. (2013) Consistent geological-simulation modeling in carbonate reservoirs, a case study from the Khuff Formation, Persian Gulf. *Journal of Petroleum Science and Engineering* 109:260–279. DOI: https://doi.org/10.1016/j.petrol.2013.07.010.

Bashari A. (2005) Khuff formation Permian-Triassic carbonate in the Qatar-South Fars arch hydrocarbon province of the Persian Gulf. *First Break* 23:43–50.
DOI: https://doi.org/10.3997/1365-2397.23.1089.26737.

Berner R. A. (2002) Examination of hypotheses for the Permo-Triassic boundary extinction by carbon cycle modeling. *Proceedings of the National Academy of Science* 99 (7): 4172–4177.
DOI: https://doi.org/10.1073/pnas.032095199.

Burchette T. P., Wright V. P. (1992) Carbonate ramp depositional systems. *Journal of Sedimentary Geology* 79:3–57.
DOI: https://doi.org/10.1016/0037-0738(92)90003-a.

Davoodi S., Asadolahi Shad S., Tavakoli V. (2024) A fresh look at the Lucia classification using mud- and grain-dominated reservoirs of the Persian Gulf. *Geoenergy Science and Engineering* 232 (212437)
DOI: https://doi.org/10.1016/j.geoen.2023.212437.

Dickson J. A. D. (1965) A modified staining technique for carbonate in the thin section. *Journal of Nature* 205:587.
DOI: https://doi.org/10.1038/205587a0.

Dunham R. J. (1962) Classification of carbonate rocks according to depositional texture. *Journal of American association petroleum geologist* 1:108–121.

Ellwood B. B., Wardlaw B. R., Nestell M. K., Nestel G. P., Lan L. T. P. (2017) Identifying globally synchronous Permian-Triassic boundary levels in successions in China and Vietnam using Graphic Correlation. *Palaeogeography, palaeoclimatology, Palaepecology* 485:561–571. DOI: https://doi.org/10.1016/j.palaeo.2017.07.012.

Embry A. F., Johannessen E. P. (1993) T-R sequence stratigraphy, facies analysis and reservoir distribution in the uppermost Triassic-Lower Jurassic succession, western Sverdrup Basin, Arctic Canada. *Arctic Geology and Petroleum Potential* 2:121–146.
DOI: https://doi.org/10.1016/b978-0-444-88943-0.50013-7.

Flugel E. (2020) Microfacies of carbonate rocks: analysis, interpretation and application. *Springer-verlag,* 976.
DOI: https://doi.org/10.1007/978-3-642-03796-2-11.

Fontana S., Nader F. H., Morad S., Ceriani A., Al-Aasm I. S. (2012) Diagenesis of the Khuff Formation (Permian-Triassic), Northern United Arab Emirates. *Journal of Arab Geoscience,* 95–111.
DOI: https://doi.org/10.1007/978-3-642-30609-9-10.

Garbelli C., Angiolini L., Brand U., Shen S., Jadoul F., Posenato R., Azmy K., Cao C. (2016) Neotethys seawater chemistry and temperature at the dawn of the end Permian mass extinction. *Gondwana Research* 35:272–285. DOI: https://doi.org/10.1016/j.gr.2015.05.012.

Ghasemi M., Kakemem U., Husinec A. (2022) Automated approach to reservoir zonation: A case study from the Upper Permian Dalan (Khuff) carbonate ramp, Persian Gulf. *Journal of Natural Gas Science and Engineering* 97:104332.
DOI: https://doi.org/10.1016/j.jngse.2021.104332.

Haghighat N., Hashemi H., Tavakoli V. (2020) Permian-Triassic extinction pattern revealed by foraminifers and geochemical records in the central Persian Gulf, southern Iran. *Palaeogeography, Palaeoclimatology, Palaeoecology* 543:109588.
DOI: https://doi.org/10.1016/j.palaeo.2020.109588.

Haq B. U. (2018) Triassic Eustatic Variations Reexamined. *The Geological Society of America* 28 (12): 4–9.
DOI: https://doi.org/10.1130/gsatg381a.1.

Haq B. U., Shutter S. R. (2008) A Chronology of Paleozoic Sea-Level Changes. *Science* 322:64–68.
DOI: https://doi.org/10.1126/science.1161648.

Heydari E., Arzani N., Hassanzadeh J. (2008) Mantle plume: The invisible serial killer-Application to the Permian-Triassic boundary mass extinction. *Palaeogeography, Palaeoclimatology, Palaeoecology* 264:147–162.
DOI: https://doi.org/10.1016/j.palaeo.2008.04.013.

Heydari E., Wade W., Hassanzadeh J. (2001) Diagenetic origin of carbon and oxygen isotope compositions of Permian-Triassic boundary strata. *Sedimentary Geology* 143 (3-4): 191–197.
DOI: https://doi.org/10.1016/s0037-0738(01)00095-1.

Hosseinzadeh M., Tavakoli V. (2024) Analyzing the impact of geological features on reservoir heterogeneity using heterogeneity logs: A case study of Permian reservoirs in the Persian Gulf. *Geoenergy Science and Engineering* 237:212810.
DOI: https://doi.org/10.1016/j.geoen.2024.212810.

——— (2025) Introducing an innovative method for assessing reservoir heterogeneity using Zenga index in the Permian Basin of the central Persian Gulf. *SPE Journal* 30 (5): 2587–2602.
DOI: https://doi.org/10.2118/225454-PA.

Huang Y., Chen Z., Algeo T., Zhao L., Baud A., Bhat G. M., Zhang L., Guo Z. (2019) Two-stage marine anoxia and biotic response during the Permian-Triassic transition in Kashmir, northern India: pyrite framboid evidence. *Global and Planetary Change* 172:124–139.
DOI: https://doi.org/10.1016/j.gloplacha.2018.10.002.

Insalaco E., Virgone A., Courme B., Gaillot J., Kamali M., Moallemi M. A. andLotfpour, Monibi S. (2006) Upper Dalan Member and Kangan Formation between the Zagros Mountains and offshore Fars, Iran: depositional system, biostratigraphy and stratigraphic architecture. *Journal of GeoArabia* 11:75–176.
DOI: https://doi.org/10.2113/geoarabia110275.

Jafarian A., Javanbakht M., Koeshidayatullah A., Pimentel N., Salad Hersi O., Yahyaei A., Beigi M. (2017) Paleo environmental, diagenetic, and eustatic controls on the Permo-Triassic carbonate-evaporate reservoir quality, Upper Dalan and Kangan formations, Lavan Gas Field, Zagros Basin. *Journal of Geological* 53:1442–1457.
DOI: https://doi.org/10.1002/gj.2965.

Jamalian A., Tavakoli V. (2022) Heterogeneity evaluation of pore types based on dipole shear sonic imager logs by means of statistical parameters, the central Persian Gulf. *Geophysical Prospecting* 70 (9): 1565–1579. DOI: https://doi.org/10.1111/1365-2478.13262.

Jehangir Khan M., Ghazi S., Mehmood M., Yazdi A., Naseem A. A., Serwar U., Zaheer A., Ullah H. (2021) Sedimentological and provenance analysis of the Cretaceous Moro formation Rakhi Gorge, Eastern Sulaiman Range, Pakistan. *Iranian Journal of Earth Sciences* 13 (4): 252–266.
DOI: https://doi.org/10.30495/ijes.2021.1917721.1564.

Jodeyri-Agaii R., Rahimpour-Bonab H., Tavakoli V., Kadkhodaie-Ilkhchi R., Yousefpour M. R. (2018) Integrated approach for zonation of a mid-Cenomanian carbonate reservoir in a sequence stratigraphic framework. *Geologica Acta* 16 (3): 321–337.
DOI: https://doi.org/10.1344/GeologicaActa2018.16.3.5.

Kakemem U., Ghasemi M., Adabi M. H., Husinec A., Mahmoudi A., Anderskouv K. (2023) Sedimentology and sequence stratigraphy of automated hydraulic flow units-The Permian Upper Dalan Formation, Persian Gulf. *Marine and petroleum geology* 147:105965.
DOI: https://doi.org/10.1016/j.marpetgeo.2022.105965.

Kakemem U., Jafarian A., Husinec A., Adabi M. H., Mahmoudi A. (2021) Facies, sequence framework, and reservoir quality along a Triassic carbonate ramp: Kangan Formation, South Pars Field, Persian Gulf Superbasin. *Journal of Petroleum Science and Engineering* 198:108166. DOI: https://doi.org/10.1016/j.petrol.2020.108166.

Karimi H., Kohansal G. N., Kangazian A. (2015) Sedimentary Environment and Sequence Stratigraphy of the Kangan Formation in Kish Gas Field (Kish Well A1 Subsurface Section). *Journal of Science and Technology* 8:655–663.
DOI: https://doi.org/10.17485/ijst/2015/v8i7/62853.

Kaveh-Ahangar S., Nozaem R., Tavakoli V. (2023) The effects of planar structures on reservoir quality of Triassic Kangan formation in the central Persian Gulf, an integrated approach. *Journal of African Earth Sciences* 197:104764.
DOI: https://doi.org/10.1016/j.jafrearsci.2022.104764.

Khalifa M. A. (2005) Lithofacies, diagenesis and cyclicity of the 'Lower Member' of the Khuff Formation (Late Permian), Al Qasim Province, Saudi Arabia. *Journal of Asian Earth Sciences* 25:719–734. DOI: https://doi.org/10.1016/j.jseaes.2004.05.008.

Lucia F. J. (2007) Carbonate Reservoir Characterization. *Springer-Verlag, Berlin,* 341. DOI: https://doi.org/10.1007/978-3-540-72742-2.

Maaleki-Moghadam M., Rafiei B., Richoz S., Woods A. D., Krystyn L. (2019) Anachronistic facies and carbon isotopes during the end-Permian biocrisis: Evidence from the mid-Tethys (Kisejin, Iran). *Palaeogeorraphy, Palaeoclimatology, Palaeocology* 516:364–383. DOI: https://doi.org/10.1016/j.palaeo.2018.12.007.

Mehrabi H., Rahimpour-Bonab H., Enayati-Bidgoli A. H., Esrafili-Dizaji B. (2015) Impact of contrasting paleoclimate on carbonate reservoir architecture: Cases from arid Permo-Triassic and humid Cretaceous in the south and southwestern Iran. *Journal of Petroleum Science and Engineering* 126:262–283. DOI: https://doi.org/10.1016/j.petrol.2014.12.020.

Moeini M., Rahimpour-Bonab H., Tavakoli V. (2023) Evidence for Isolated Platform Development in the Cenomanian on the Passive Margin of Neotethys, Southwest Iran. *Minerals* 13 (6) DOI: https://doi.org/10.3390/min13060757.

Mohsin M., Tavakoli V., Jamalian A. (2023) The effects of heterogeneity on pressure derived porosity changes in carbonate reservoirs, Mishrif formation in SE Iraq. *Petroleum Science and Technology* 41 (8): 898–915. DOI: https://doi.org/10.1080/10916466.2022.2070210.

Moore C. H. (2001) Carbonate reservoirs: porosity evolution and diagenesis in a sequence stratigraphic framework, Amsterdam. *Elsevier* 55:1–444. DOI: https://doi.org/10.1016/s0070-4571(01)80001-7.

Naderi-Khujin M., Seyrafian A., Vaziri-Moghaddam H., Tavakoli V. (2016a) A record of global change: OAE 1a in Dariyan shallow-water platform carbonates, southern Tethys, Persian Gulf, Iran. *Facies* 62 (4): 25. DOI: https://doi.org/10.1007/s10347-016-0476-6.

——— (2016b) Characterization of the late Aptian top-Dariyan disconformity surface offshore SW Iran: a multi-proxy approach. *Journal of Petroleum Geology* 39 (3): 269–286. DOI: https://doi.org/10.1111/jpg.12646.

Naderi-Khujin M., Tavakoli V. (2023) Composition, environment, and economic value of the Permian to Cretaceous coated grains from Zagros and the Persian Gulf. *International Journal of Sediment Research* 38 (3): 316–334. DOI: https://doi.org/10.1016/j.ijsrc.2022.12.004.

Naderi-Khujin M., Tavakoli V., Seyrafian A., Vaziri-Moghaddam H. (2020) How a mud-dominated ramp changed to a carbonate–clastic oil reservoir: Sea-level fluctuations in cretaceous of the central Persian Gulf. *Marine and Petroleum Geology* 116:104301. DOI: https://doi.org/10.1016/j.marpetgeo.2020.104301.

Nafisi F., Tavakoli V. (2023) The role of textural parameters of industrial core CT scan images in detecting the petrophysical characteristics of carbonate reservoirs, Permian Dalan Formation, the central Persian Gulf. *Geoenergy Science and Engineering* 230:212277. DOI: https://doi.org/10.1016/j.geoen.2023.212277.

Nazari M. H., Tavakoli V., Rahimpour-Bonab H., Sharifi-Yazdi M. (2019) Investigation of factors influencing geological heterogeneity in tight gas carbonates, Permian reservoir of the Persian Gulf. *Journal of Petroleum Science and Engineering* 183 (1): 106341. DOI: https://doi.org/10.1016/j.petrol.2019.106341.

Nazemi M., Tavakoli V., Rahimpour-Bonab H., Hosseini M., Sharifi-Yazdi M. (2018) The effect of carbonate reservoir heterogeneity on Archie's exponents (a and m), an example from Kangan and Dalan gas formations in the central Persian Gulf. *Journal of Natural Gas Science and Engineering* 59:297–308. DOI: https://doi.org/10.1016/j.jngse.2018.09.007.

Nazemi M., Tavakoli V., Rahimpour-Bonab H., Sharifi-Yazdi M. (2021) Integrating petrophysical attributes with saturation data in a geological framework, Permian–Triassic reservoirs of the central Persian Gulf. *Journal of African Earth Sciences* 179:104203. DOI: https://doi.org/10.1016/j.jafrearsci.2021.104203.

Prothero D. R., Schwab F., Schwab L. F. (1996) Sedimentary Geology: An introduction to sedimentary rocks and stratigraphy. *W.H. Freeman* 575 DOI: https://doi.org/10.1016/s0037-0738(97)84049-3.

Rafiei M., Rahimpour-Bonab H., Tavakoli V., Khorasani E. (2016) Quantifying sedimentary and diagenetic controls on fracturing: An application in rock engineering systems. *Journal of Geophysics and Engineering* 13 (6): 928–939. DOI: https://doi.org/10.1088/1742-2132/13/6/928.

Rahimpour-Bonab H., Enayati-Bidgoli A. H., Navidtalab A., Mehrabi H. (2014) Appraisal of intra reservoir barriers in the Permo-Triassic successions of the Central Persian Gulf, Offshore Iran. *Geologica Acta* 12 (1): 87–107. DOI: https://doi.org/10.1344/105.000002076.

Read J. F. (1985) Carbonate Platform Facies Models. *AAPG Bulletin* 69 (1): 1–21. DOI: https://doi.org/10.1306/ad461b79-16f7-11d7-8645000102c1865d.

Reading H. G. (1996) Sedimentary environments: processes, facies and stratigraphy. *3rd Blackwell,* 688.

Rezavand N., Jahani D., Asilian H. (2017) Facies, Depositional Environment and Sequence Stratigraphy of Dalan Formation in Persian Gulf (Qatar-South Fars Arch) Well SP-A Subsurface Section. *Journal of Science and Technology* 10 (3): 1–16. DOI: https://doi.org/10.17485/ijst/2017/v10i34/88678.

Saitoh M., Isozaki Y. (2021) Carbon Isotope Chemostratigraphy across the Permian-Triassic Boundary at Chaotian, China: Implications for the Global Methane Cycle in the Aftermath of the Extinction. *frontier in earth science* 8:596178. DOI: https://doi.org/10.3389/feart.2020.596178.

Sarg J. F. (1988) Carbonate sequence stratigraphy, In Wilgus, C.K. et al. (eds.), Sea-level changes: an integrated approach. *SEPM Special publication,* 155–181. DOI: https://doi.org/10.2110/pec.88.01.0155.

Shabani F., Amini A., Tavakoli V., Chehrazi A., Gong C. (2023) 3D basin and petroleum system modelling of the early cretaceous play in the NW Persian Gulf. *Geoenergy Science and Engineering* 226:211768. DOI: https://doi.org/10.1016/j.geoen.2023.211768.

Shabani F., Amini A., Tavakoli V., Honarmand J., Gong C. (2022) 3D forward stratigraphic modeling of the Albian succession in a part of the northeastern margin of the Arabian Plate and its implications for exploration of subtle traps. *Marine and Petroleum Geology* 145 (105880) DOI: https://doi.org/10.1016/j.marpetgeo.2022.105880.

Sharifi-Yazdi M., Rahimpour-Bonab H., Nazemi M., Tavakoli V., Gharechelou S. (2020) Diagenetic impacts on hydraulic flow unit properties: insight from the Jurassic carbonate Upper Arab Formation in the Persian Gulf. *Journal of Petroleum Exploration and Production Technology* 10 (5): 1783–1802. DOI: https://doi.org/10.1007/s13202-020-00884-7.

Sharifi-Yazdi M., Rahimpour-Bonab H., Tavakoli V., Nazemi M., Kamali M. R. (2019) Linking diagenetic history to depositional attributes in a high-frequency sequence stratigraphic framework: A case from upper Jurassic Arab formation in the central Persian Gulf. *Journal of African Earth Sciences* 153:91–110. DOI: https://doi.org/10.1016/j.jafrearsci.2019.02.006.

Sharland P. R., Archer R., Casey D. M., Davies R. B., Hall S. H., Heward A. P., Horbury A. D., Simmons M. D. (2001) Arabian Plate Sequence Stratigraphy. *Journal of GeoArabia Special Publication,* 2371. DOI: https://doi.org/10.2113/geoarabia0901199.

Shinn E. A. (1983) Birdseyes, fenestrae, shrinkage pores and loferites: a reevaluation. *Journal of Sedimentary Research* 53:619–629. DOI: https://doi.org/10.1306/212f8247-2b24-11d7-8648000102c1865d.

Soleimani A., Tavakoli V. (2024) Deep Dive into the factors influencing acoustic velocity in the Dalan-Kangan formations, the central Persian Gulf. *Geoenergy Science and Engineering* 235 (212739) DOI: https://doi.org/10.1016/j.geoen.2024.212739.

Szabo F., Kheradpir A. (1978) Permian and Triassic stratigraphy, Zagros basin, southwest Iran. *Journal of Petroleum Geology* 2:57–82. DOI: https://doi.org/10.1111/j.1747-5457.1978.tb00611.x.

Tavakoli V. (2017) Application of gamma deviation log (GDL) in sequence stratigraphy of carbonate strata, an example from offshore Persian Gulf, Iran. *Journal of Petroleum Science and Engineering* 156:868–876. DOI: https://doi.org/10.1016/j.petrol.2017.06.069.

——— (2015) Chemostratigraphy of the Permian-Triassic Strata of the Offshore Persian Gulf, Iran. *Chemostratigraphy: Concepts, Techniques, and Applications,* 373–393.
DOI: https://doi.org/10.1016/b978-0-12-419968-2.00014-5.

——— (2021) Permeability's response to dolomitization, clues from Permian–Triassic reservoirs of the central Persian Gulf. *Marine and Petroleum Geology* 123:104723.
DOI: https://doi.org/10.1016/j.marpetgeo.2020.104723.

Tavakoli V., Hassani H. Mondak A. D. Rahimpour-Bonab (2022) How petrophysical heterogeneity controls the saturation calculations in carbonates, the Barremian–Aptian of the central Persian Gulf. *Journal of Petroleum Science and Engineering* 208 (109568)
DOI: https://doi.org/10.1016/j.petrol.2021.109568.

Tavakoli V., Jamaliyan A. (2019) Porosity evolution in dolomitized Permian-Triassic strata of the Persian Gulf, insights into the porosity origin of dolomite reservoirs. *Journal of Petroleum Science and Engineering* 181 (106191)
DOI: https://doi.org/10.1016/j.petrol.2019.106191.

Tavakoli V., Naderi-Khujin M., Seyedmehdi Z. (2018) The end-Permian regression in the western Tethys: sedimentological and geochemical evidence from offshore the Persian Gulf, Iran. *Journal of GeoMarine Letters* 38 (2): 179–192.
DOI: https://doi.org/10.1007/s00367-017-0520-8.

Tomasovych A. (2004) Microfacies and depositional environment of an upper Triassic intra-platform carbonate basin: the Fatric unit of west Carpathians (Slovakia). *Facies* 50:77–105.
DOI: https://doi.org/10.1007/s10347-004-0004-y.

Tucker M. E. (2001) Sedimentary petrology. *Third edition, Blackwell, Oxford,* 260. DOI: https://doi.org/10.1017/S0016756802266510.

Tucker M. E., Wright V. P. (1990) Carbonate sedimentology. *London, Blackwell Scientific Publications* 482
DOI: https://doi.org/10.1002/9781444314175.

Warren J. K. (2006) Evaporites: sediments, resources and hydrocarbons. *Springer Verlag, Brunei,* 1035.
DOI: https://doi.org/10.1007/3-540-32344-9.

Wilson J. L. (1975) Carbonate facies in geological history. *Springer, Berlin-Heidelberg, New York,* 471.
DOI: https://doi.org/10.1007/978-1-4612-6383-8.

Ying C., Antoine B., Jianxin Y., Lee R. K., Katherine H. F., Shangguo S., Vivi V. (2017) Carbon cycle perturbation expressed in terrestrial Permian–Triassic boundary sections in South China. *Global and Planetary Change* 148:272–285.
DOI: https://doi.org/10.1016/j.gloplacha.2015.10.018.

Zhao H., Lyu Z. H., Chen Z., Algeo T. J., Orchard M. J., Liu Y., Hu Z., Zhang L., Xiumei Zhang X. (2021) Integrated biochemostratigraphy of the Permian-Triassic boundary beds in a shallow carbonate platform setting (Yangou, South China) *Global and planetary change* 206 (1-2) DOI: https://doi.org/10.1016/j.gloplacha.2021.103583.